


# Electrochemical Dealloying Preparation and Morphology Evolution of Nanoporous Au with Enhanced SERS Activity

Fei Li <sup>1,†</sup>, Silang Luo <sup>2,3,†</sup>, Fengsheng Qu <sup>2</sup>, Dou Wang <sup>2</sup>, Chao Li <sup>3,\*</sup> and Xue Liu <sup>2,\*</sup> 

<sup>1</sup> School of Mechatronics and Rail Transportation, Zhejiang Fashion Institute of Technology, Ningbo 315211, China

<sup>2</sup> Institute of Materials, China Academy of Engineering Physics, Mianyang 621908, China

<sup>3</sup> School of Materials Science and Engineering, Harbin University of Science and Technology, Harbin 150040, China

\* Correspondence: lichao@hrbust.edu.cn (C.L.); xueliuthu@126.com (X.L.);

Tel.: +86-0335-8074631 (C.L.); +86-028-65726372 (X.L.)

† These authors contributed equally to this work.

**Abstract:** Nanoporous Au (NPG) prepared by dealloying is one of the most used substrates for surface-enhanced Raman scattering (SERS). The morphology tailoring of the NPG to obtain both ultrafine pores and suitable Au/Ag ratio is of great importance for the acquiring of enhanced SERS performance. Compared with the chemical dealloying, the electrochemical dealloying can tailor the NPG to be more flexible by the additional adjustment of dealloying voltage and current. Thus, further understanding on the morphology evolution of NPG during the electrochemical dealloying to obtain enhanced SERS performance is of great importance. In the presented work, the morphology and composition evolution of the NPG film during the electrochemical dealloying was investigated. NPG films with a stable pore diameter of approximately 11 nm as well as diverse compositions were obtained by electrochemical dealloying an Au-Ag alloy film. The prepared NPG film exhibits an enhanced SERS activity with an enhancement factor (*EF*) of  $7.3 \times 10^6$  and an excellent detection limit of  $10^{-9}$  M. This work provides insights into the morphology and composition evolution of the NPG during the electrochemical dealloying process to obtain enhanced SERS performance.

**Keywords:** nanoporous gold; sputtering; electrochemical dealloying; morphology evolution; SERS



**Citation:** Li, F.; Luo, S.; Qu, F.; Wang, D.; Li, C.; Liu, X. Electrochemical Dealloying Preparation and Morphology Evolution of Nanoporous Au with Enhanced SERS Activity. *Coatings* **2023**, *13*, 489. <https://doi.org/10.3390/coatings13030489>

Academic Editor: Angela De Bonis

Received: 5 January 2023

Revised: 18 January 2023

Accepted: 27 January 2023

Published: 22 February 2023



**Copyright:** © 2023 by the authors. Licensee MDPI, Basel, Switzerland. This article is an open access article distributed under the terms and conditions of the Creative Commons Attribution (CC BY) license (<https://creativecommons.org/licenses/by/4.0/>).

## 1. Introduction

It is of great importance to recognize and detect trace molecule in medicine, catalysis, and material sciences [1,2]. Surface-enhanced Raman scattering (SERS) provides a high-precision alternative technique to achieve this goal [3–6]. Electromagnetic enhancement and chemical enhancement are the two main mechanisms for the origin of the SERS activity [7]. The electromagnetic enhancement is mainly caused by the localized electromagnetic field of the surface plasmon resonance (SPR), and the chemical enhancement is mainly induced by the charge transfer between the adsorbed molecule and the SERS substrate [7–9]. Commonly, the electromagnetic enhancement is much higher than the chemical enhancement [9]. The electromagnetic enhancement on the whole SERS substrate is usually not uniform, and the areas with high electromagnetic enhancement are usually called “hot spots”, where the localized electromagnetic fields are achieved [10,11]. The hot spots are affected by the size, distance, distribution, and the shape of the particles. Especially, the shape and arrangement of the particles are most important, and the hot spots are usually created by sub-10-nm gaps or sharp edges [3,7,12]. Au, Ag, and Cu exhibit better SERS activity than the other metals, but the Ag and Cu are easier to oxidize than Au. Thus, nanoporous Au (NPG) is one of the most widely used substrates due to its excellent and stable SERS activities [13–15]. To obtain better SERS performance, it is of great importance to investigate the morphology evolution to achieve the controllable adjustment of the pore size of the NPGs.

Chemical dealloying is one of the most employed methods for preparing NPG films [16,17]. By changing the dealloying time, temperature, and solution concentration, the morphology of the NPG can be adjusted, and relatively high SERS performance can be obtained. For example, Xue [18] et al. reported the detection limit of  $10^{-6}$  M of NPG by dealloying an Au-based metallic glass. Hu [16] et al. obtained a high enhancement factor (*EF*) of  $2.4 \times 10^5$  by dealloying an Au-Ag alloy. By employing electrochemical dealloying, the morphology of the NPG can be further effectively adjusted by introducing new controllable variables of potential and current [19]. This will benefit the improvement of the SERS performance of the NPG. In addition to that, the dealloying speed can be promoted due to the applied potential. However, the morphology evolution of the NPG during electrochemical dealloying is still lacked.

In the presented work, NPG films with fine pore diameters of approximately 11 nm were obtained by electrochemical dealloying a sputtered Au-Ag film. The dealloying morphology and composition evolution of the prepared NPG films were investigated. Enhanced SERS activity with an enhancement factor (*EF*) of  $7.3 \times 10^6$  and detection limit of  $10^{-9}$  M was obtained. This work provides insights into the morphology and composition evolution of the NPG during the electrochemical dealloying process to obtain enhanced SERS performance.

## 2. Experimental Methods

It has been reported that the dealloying processing cannot occur when the content of the noble element is too high, and the dealloying will collapse when the content of the noble element is too low [20,21]. Thus, Au<sub>40</sub>Ag<sub>60</sub> was selected to be the precursor alloy. Au-Ag film with thickness of  $\sim 1$   $\mu\text{m}$  was sputtered on the (100) plane of a Si wafer with an Au<sub>40</sub>Ag<sub>60</sub> target under an Ar atmosphere of 1.1 Pa and an electric current of 0.1 A. The Si wafer was previously coated by a Cr transition layer with thickness of  $\sim 20$  nm by sputtering. The detailed procedures can be found elsewhere [16]. Au-Ag film samples with areas of  $\sim 10 \times 10$  mm<sup>2</sup> were used for electrochemical dealloying. A standard three-electrode electrochemical cell with a Hg/HgSO<sub>4</sub> reference electrode and platinum counter electrode was used to perform the electrochemical dealloying in 0.5 mol/L nitric acid solution. To promote the diffusion of the Au atoms to obtain NPG, the dealloying temperature was set to be 288 K. The samples were first subjected to potentiodynamic polarization, with a potential sweep rate of 1 mV/s to determine the dealloying potentials, then electrochemical dealloying under a different potential for a different time to acquire NPG films.

The structure of the sputtered and dealloyed samples were inspected by X-ray diffraction (XRD, D/max-RB, Rigaku, Tokyo, Japan). The scanning rate was  $8^\circ \text{min}^{-1}$  and the detecting step was  $0.02^\circ$ . The obtained XRD curves were indexed by a PDF database through the Jade 6. The morphology of the samples was examined by a scanning electron microscope (SEM, LEO-1530, Zeiss, Oberkochen, Germany) with an operating voltage of 10 kV, and the compositions of the dealloyed NPG samples were inspected by energy disperse X-ray spectroscopy (EDS, X-act, Oxford, UK) with an operating voltage of 20 kV. The diameters of the pores were statistically measured by employing Image Pro (Plus6.0). The standard deviation was calculated by the measured data. Analytically purity Rhodamine B (RhB) was purchased from Sinopharm Chemical Reagent Co., Ltd. (Shanghai, China). The SERS measurement was carried out using the RhB as the probe molecule. RhB aqueous solution with volume of 2  $\mu\text{L}$  was dropped on the as-sputtered Au-Ag film and the NPG samples, respectively, and then dried at 323 K for 30 min in atmosphere. Then, SERS spectra were measured in the center of the droplet by a self-designed microscopic confocal Raman spectrometer. A charge-coupled device (CCD) detector (ivac-316, Andor, Belfast, UK) with a resolution of  $1 \text{ cm}^{-1}$  was used to collect the Raman signal. The applied excitation laser wavelength was 532 nm, the laser power was 5 mW, and the diameter of the laser beam was  $\sim 5$   $\mu\text{m}$ . A scan time of 0.5 s, field lens of fifty times, and accumulation of five times were applied during the SERS measurements.

### 3. Results and Discussion

Figure 1a shows the XRD diffractogram of the as-prepared sample. Peaks sitting at  $2\theta = 38^\circ, 45^\circ, 69^\circ, 78^\circ$ , and  $82^\circ$  were observed. After indexing, it was found that the peak sitting at  $2\theta = 69^\circ$  corresponded to the (400) plane of silicon, and the other peaks were very close to the feature peaks of Ag and Au but with a little shift. Since there was no obvious separation in these peaks, it can be concluded that these peaks should correspond to the Au-Ag alloy. The lone appearance of the peak at  $2\theta = 69^\circ$  for silicon should have been caused by the employment of the single-crystal Si substrate. Due to the texturing effect, only the peak corresponding to the (400) plane was observed. The intensity of this peak was quite weak compared with our previous work [16]. This phenomenon may be caused by the relatively thicker Au-Ag film and the defects in the Si wafer.

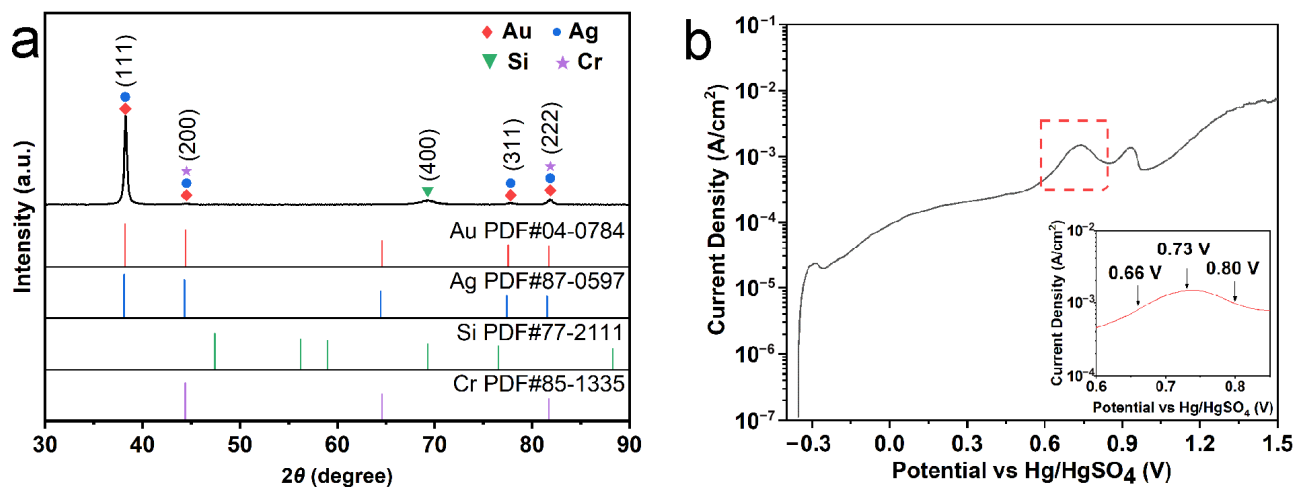


**Figure 1.** Characterization of the as-prepared Au-Ag film. (a) XRD diffractogram. (b) Potentiodynamic polarization curve.

Two peaks sitting at 0.74 V and 0.93 V were observed in the potentiodynamic polarization curve of the Au-Ag film (Figure 1b). According to the previous report, these two peaks correspond to the oxidation of constituted elements with different oxidation potentials [22]. Therefore, the peak sitting at 0.74 V corresponds to the oxidation of Ag, and the other peak corresponds to the oxidation of Au. According to the potentiodynamic polarization curve, 0.66 V, 0.73 V, and 0.80 V were selected as the electrochemical dealloying potentials. The dealloying parameters are listed in Table 1.

**Table 1.** Chemical dealloying parameters for the samples.

| Sample No. | Dealloying Potential (V) | Dealloying Time (min) |
|------------|--------------------------|-----------------------|
| 1          | 0.66                     | 2                     |
| 2          | 0.66                     | 5                     |
| 3          | 0.66                     | 15                    |
| 4          | 0.73                     | 5                     |
| 5          | 0.80                     | 5                     |

According to Figure 2a, the Au-Ag film was quite dense, and no obvious pores or cracks were observed, but some granular structure can be observed, which is a typical morphology of the sputtered surface [23]. Very fine nanopores form after dealloying under 0.66 V for 2 min. The average pore diameter was measured to be  $10 \pm 6$  nm. With extending the dealloying time or increasing the dealloying potential, the average diameter of the pores kept stable around 10–12 nm, while the density of the pores increased and cracks started

to form. The cracks may have been induced by the stress created during the dealloying processes [24–27].

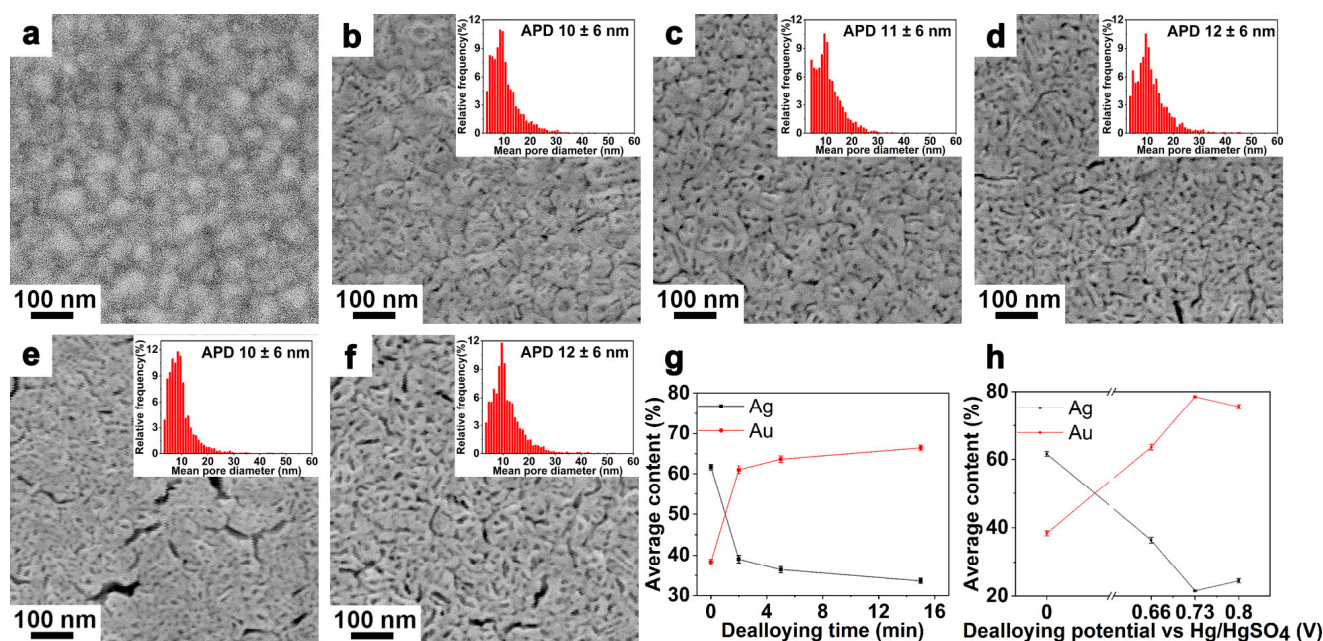


**Figure 2.** SEM images and composition variation of the dealloyed samples. (a) SEM image of the Au-Ag film. (b–f) SEM images of the 1#–5# samples with the statistical analysis of the pore diameter in the insert, respectively. (g) Composition variation of the dealloyed sample against the dealloying time. (h) Composition variation of the dealloyed sample against the dealloying potential.

The composition of the as-sputtered alloy is measured to be  $\sim\text{Au}_{32}\text{Ag}_{68}$  by EDS. As shown in Figure 2g,h, the content of Au in the porous film rapidly increases in the very early stage of the dealloying, then increases slowly and gradually turns stable with the extending dealloying time. The composition variation tendency is very similar to that in chemical dealloying [16]. With increasing the dealloying potential, the content of Au in the porous film also rapidly increases when the potential is less than 0.73 V, while further increasing the dealloying potential results in a decrease of Au content. According to Figure 1b, it can be found that the polarization current starts to drop when the potential exceeds 0.73 V. Since the peak sitting at 0.74 V corresponds to the oxidation of Ag, the current dropping means the reducing of Ag oxidation. In addition to that, the potential 0.8 V is close to the oxidation peak of Au (0.93 V). Thus, Au may also be oxidized and dissolved at 0.8 V. The reducing oxidation as well as the oxidation of Au together lead to the decreasing of Au in the nanoporous film under high dealloying potential.

Figure 3 shows the SERS spectra of the dealloyed samples with  $10^{-5}$  M RhB adsorbed. According to the previous literature [3,28,29], the main shifts of the RhB molecule were indexed, and the results are listed in Table 2. The intensity of the feature shifts ( $@1646\text{ cm}^{-1}$ ) increases with extending the dealloying time (1#, 2#, and 3# samples). The composition and the number of hot spots are the main affected factors to determine the SERS activity of the substrate. The hot spots are commonly contributed by the sub-10-nm gaps [3,16]. It can be seen from Figure 2 that the density of the fine nanopores increases with the dealloying, which may lead to the increasing of hot spots. The newly formed cracks may also create some new hot spots. In addition to that, the Au content also increases with the dealloying time. Due to the relatively easy oxidation of Ag [3,25,26], the increasing of Au content in the Au-Ag substrate improves the SERS performance. It is also noticed that the SERS activity of the sample first increases and then decreases with the increasing dealloying potential (2#, 4#, and 5# samples). The decreasing SERS activity may be caused by the decreasing Au content under high dealloying potential.

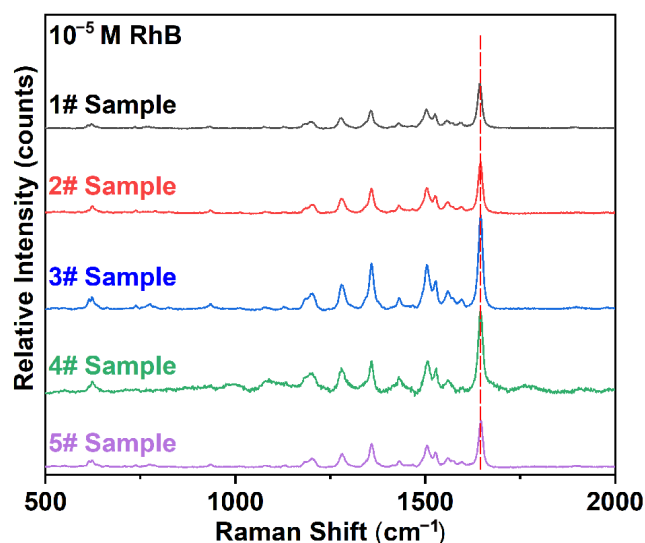


**Figure 3.** SERS spectra of the electrochemical dealloyed samples dealloyed for different times with  $10^{-5}$  M RhB adsorbed.

**Table 2.** Experimental and the literature SERS shifts of RhB molecules.

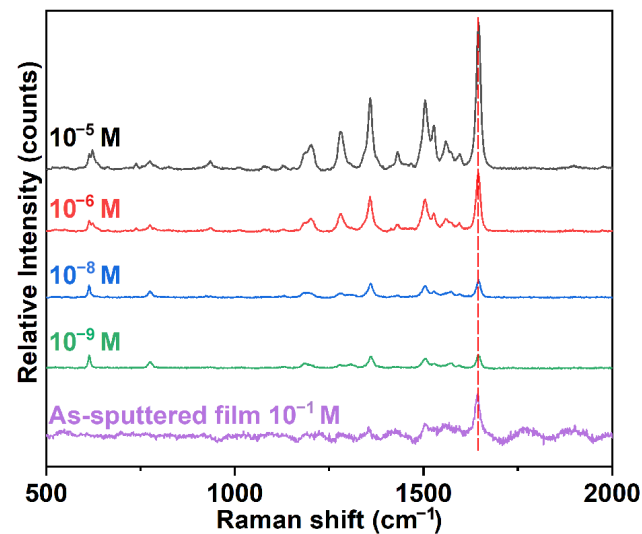
| Raman Shift ( $\text{cm}^{-1}$ ) |              | Assignments [3,28,29]       |
|----------------------------------|--------------|-----------------------------|
| Literature [3,28,29]             | Experimental |                             |
| 619                              | 619          | Aromatic bending            |
| 776                              | 776          | C-H out of plane            |
| 933                              | 934          | -                           |
| 1009                             | 1012         | -                           |
| 1080                             | 1085         | -                           |
| 1132                             | 1130         | C-H in plane                |
| 1195                             | 1196         | Aromatic C-H bending        |
| 1275                             | 1280         | C-C bridge bands stretching |
| 1356                             | 1359         | Aromatic C-C stretching     |
| 1433                             | 1433         | -                           |
| 1507                             | 1506         | Aromatic C-C stretching     |
| 1526                             | 1527         | -                           |
| 1563                             | 1564         | Aromatic C-C stretching     |
| 1596                             | 1595         | C=C stretching              |
| 1648                             | 1646         | Aromatic C-C stretching     |

Figure 4 shows the SERS spectra of RhB with concentrations from  $10^{-5}$  M to  $10^{-9}$  M on 3# sample. The intensity of the Raman shifts keeps decreasing with decreasing RhB concentration. After the Lorentz fitting, the intensities of the Raman shift @1646  $\text{cm}^{-1}$  were measured. As listed in Table 3, the intensity of the Raman shifts of RhB concentrations of  $10^{-5}$  M,  $10^{-6}$  M,  $10^{-8}$  M, and  $10^{-9}$  M were 17,795 counts, 6137 counts, 2279 counts, and 1243 counts, respectively. Thus, the detection limit of the sample was lower than  $10^{-9}$  M, which was much better than the previous reports [16,30,31]. The Raman spectrum of the Au-Ag film with  $10^{-1}$  M RhB adsorbed was also measured, as shown in Figure 4.

The SERS activity of the substrate can be evaluated by  $EF$ , which is usually calculated by the formula [3,12,16]:

$$EF = (I_{\text{SERS}}/N_{\text{SERS}})/(I_{\text{R}}/N_{\text{R}}) \quad (1)$$

where  $I_{\text{SERS}}$  and  $I_{\text{R}}$  are the intensities of the Raman shifts in the SERS and bulk Raman spectra, respectively, and  $N_{\text{SERS}}$  and  $N_{\text{R}}$  are the number of probe molecules contributing to the SERS signal and the bulk Raman signal, respectively.



**Figure 4.** SERS spectra of RhB with different concentrations on the 3# sample and SERS diffractogram of RhB with  $10^{-1}$  mol/L RhB on the Au-Ag film.

**Table 3.** EF of the 3# with different RhB concentrations.

| Spectra                 | Area (mm <sup>2</sup> ) | C <sub>RhB</sub> (mol·L <sup>-1</sup> ) | Average Intensity @1646 cm <sup>-1</sup> | EF                |
|-------------------------|-------------------------|---|--|-------------------|
| 3# Sample               | 14.2                    | $10^{-5}$                               | 17,795                                   | $1.0 \times 10^4$ |
|                         | 14.0                    | $10^{-6}$                               | 6137                                     | $3.5 \times 10^4$ |
|                         | 13.1                    | $10^{-8}$                               | 2279                                     | $1.2 \times 10^6$ |
|                         | 14.6                    | $10^{-9}$                               | 1243                                     | $7.3 \times 10^6$ |
| As-sputtered Au-Ag film | 41.2                    | $10^{-1}$                               | 5994                                     | -                 |

Since the SERS tests are prepared under the same conditions, the equation can be written as:

$$EF = (I_{\text{SERS}}/I_{\text{R}}) \cdot (C_{\text{R}}/C_{\text{SERS}}) \cdot (A_{\text{SERS}}/A_{\text{R}}), \quad (2)$$

where  $C_{\text{R}}$  and  $C_{\text{SERS}}$  are the concentrations of the RhB on the Au-Ag film and the dealloyed samples, respectively, and  $A_{\text{R}}$  and  $A_{\text{SERS}}$  are the RhB droplet diameter on the Au-Ag film and the dealloyed samples, respectively. According to Equation (2), it was calculated that 3# sample possesses a SERS EF as high as  $7.3 \times 10^6$ , which is much higher than the nanoporous Au prepared by chemical dealloying and the Au/MSiO<sub>2</sub>/Ag hybrid SERS substrate [16,18,30].

#### 4. Conclusions

In the presented work, the morphology and composition evolution of the NPG during the electrochemical dealloying process were investigated. By adjusting the electrochemical dealloying parameters, fine pores and enhanced SERS performance were achieved. The following conclusions can be drawn:

- (1) NPG films with a fine pore size of approximately 10~12 nm were prepared by the electrochemical dealloying of sputtered Au-Ag alloy film;
- (2) The diameter of the pores was relatively stable but the density of the pores increased with the extending dealloying time or increasing dealloying potential;
- (3) The Au content in the NPG films first rapidly increased, then slowly increased, and gradually became stable with extending the dealloying time, while it rapidly increased when the potential was less than 0.73 V, and then decreased when the potential was higher than 0.73 V;

- (4) The electrochemical dealloyed NPG films exhibited enhanced SERS activity with a high  $EF$  of  $7.3 \times 10^6$  and an excellent detection limit of  $10^{-9}$  M, which were much better than that of the NPG prepared by chemical dealloying;
- (5) This work provides insights into the morphology and composition evolution of the NPG during the electrochemical dealloying process, which can help to prepare a new substrate with enhanced SERS performance for trace molecule detection.

**Author Contributions:** Conceptualization, X.L.; methodology, F.L., S.L. and X.L.; formal analysis, F.Q. and D.W.; validation, D.W.; writing—review and editing, C.L. and X.L.; writing—original draft preparation, F.L., S.L. and X.L.; supervision, C.L. All authors have read and agreed to the published version of the manuscript.

**Funding:** This work was supported by the National Natural Science Foundation of China (Grant Nos. 51875539), the Science and Technology on Surface Physics and Chemistry Laboratory Fund (Grant No. XKFZ202005) and the Ningbo Major Project (Grant No. 2021Z093).

**Institutional Review Board Statement:** Not applicable.

**Informed Consent Statement:** Not applicable.

**Data Availability Statement:** Not applicable.

**Acknowledgments:** The authors greatly acknowledge the support from Hongwu Ye.

**Conflicts of Interest:** The authors declare no conflict of interest.

## References

1. Li, J.F.; Huang, Y.F.; Ding, Y.; Yang, Z.L.; Li, S.B.; Zhou, X.S.; Fan, F.R.; Zhang, W.; Zhou, Z.Y.; Wu, D.Y.; et al. Shell-isolated nanoparticle-enhanced Raman spectroscopy. *Nature* **2010**, *464*, 392–395. [\[CrossRef\]](#)
2. Dai, X.; Fu, W.H.; Chi, H.Y.; Mesias, V.S.; Zhu, H.N.; Leung, C.W.; Liu, W.; Huang, J.Q. Optical tweezers-controlled hotspot for sensitive and reproducible surface-enhanced Raman spectroscopy characterization of native protein structures. *Nat. Commun.* **2021**, *12*, 9. [\[CrossRef\]](#)
3. Liu, X.; Shao, Y.; Tang, Y.; Yao, K.F. Highly uniform and reproducible surface enhanced Raman scattering on air-stable metallic glassy nanowire array. *Sci. Rep.* **2014**, *4*, 5835. [\[CrossRef\]](#)
4. Chen, N.; Xiao, T.H.; Luo, Z.Y.; Kitahama, Y.; Hiramatsu, K.; Kishimoto, N.; Itoh, T.; Cheng, Z.Z.; Goda, K. Porous carbon nanowire array for surface-enhanced Raman spectroscopy. *Nat. Commun.* **2020**, *11*, 8. [\[CrossRef\]](#)
5. Guerra, F.A.E.; Aouzal, Z.; Bouabdallaoui, M.; Jadi, S.B.; Bazzaoui, E.A. Electrochemically roughened silver surface versus fractal leaf-shaped silver crystals for surface-enhanced Raman scattering investigation of polypyrrole. *J. Solid State Electrochem.* **2019**, *23*, 1811–1827. [\[CrossRef\]](#)
6. Yu, Q.; Kong, X.; Chen, C.; Kang, C.; Huang, S. Synthesis of Ag NPs layer and its application as SERS substrate in the determination of p-phenylenediamine. *J. Solid State Electrochem.* **2021**, *25*, 683–688. [\[CrossRef\]](#)
7. Shvalya, V.; Filipič, G.; Zavašnik, J.; Abdulhalim, I.; Cvelbar, U. Surface-enhanced Raman spectroscopy for chemical and biological sensing using nanoplasmonics: The relevance of interparticle spacing and surface morphology. *Appl. Phys. Rev.* **2020**, *7*, 031307. [\[CrossRef\]](#)
8. Langer, J.; Jimenez de Aberasturi, D.; Aizpurua, J.; Alvarez-Puebla, R.A.; Auguie, B.; Baumberg, J.J.; Bazan, G.C.; Bell, S.E.J.; Boisen, A.; Brolo, A.G.; et al. Present and Future of Surface-Enhanced Raman Scattering. *ACS Nano* **2020**, *14*, 28–117. [\[CrossRef\]](#)
9. Tong, L.; Zhu, T.; Liu, Z. Approaching the electromagnetic mechanism of surface-enhanced Raman scattering: From self-assembled arrays to individual gold nanoparticles. *Chem. Soc. Rev.* **2011**, *40*, 1296–1304. [\[CrossRef\]](#)
10. Liu, T.Y.; Tsai, K.T.; Wang, H.H.; Chen, Y.; Chen, Y.H.; Chao, Y.C.; Chang, H.H.; Lin, C.H.; Wang, J.K.; Wang, Y.L. Functionalized arrays of Raman-enhancing nanoparticles for capture and culture-free analysis of bacteria in human blood. *Nat. Commun.* **2011**, *2*, 538. [\[CrossRef\]](#)
11. Lan, L.L.; Gao, Y.M.; Fan, X.C.; Li, M.Z.; Hao, Q.; Qiu, T. The origin of ultrasensitive SERS sensing beyond plasmonics. *Front. Phys.* **2021**, *16*, 26. [\[CrossRef\]](#)
12. Liu, H.; Zhang, L.; Lang, X.; Yamaguchi, Y.; Iwasaki, H.; Inouye, Y.; Xue, Q.; Chen, M. Single molecule detection from a large-scale SERS-active Au<sub>79</sub>Ag<sub>21</sub> substrate. *Sci. Rep.* **2011**, *1*, srep00112. [\[CrossRef\]](#)
13. Huang, J.; He, Z.; Liu, Y.; Liu, L.; He, X.; Wang, T.; Yi, Y.; Xie, C.; Du, K. Large surface-enhanced Raman scattering from nanoporous gold film over nanosphere. *Appl. Surf. Sci.* **2019**, *478*, 793–801. [\[CrossRef\]](#)
14. Chen, C.; Liu, Z.W.; Cai, C.; Qi, Z.M. Facile fabrication of nanoporous gold films for surface plasmon resonance (SPR) sensing and SPR-based SERS. *J. Mater. Chem. C* **2021**, *9*, 6815–6822. [\[CrossRef\]](#)
15. Xue, Y.P.; Scaglione, F.; Celegato, F.; Denis, P.; Fecht, H.J.; Rizzi, P.; Battezzati, L. Shape controlled gold nanostructures on de-alloyed nanoporous gold with excellent SERS performance. *Chem. Phys. Lett.* **2018**, *709*, 46–51. [\[CrossRef\]](#)

16. Hu, L.W.; Liu, X.; Le, G.M.; Li, J.F.; Qu, F.S.; Lu, S.Y.; Qi, L. Morphology evolution and SERS activity of the nanoporous Au prepared by dealloying sputtered Au-Ag film. *Phys. B Condens. Matter* **2019**, *558*, 49–53. [\[CrossRef\]](#)
17. Haensch, M.; Graf, M.; Wang, W.J.; Nefedov, A.; Woll, C.; Weissmuller, J.; Wittstock, G. Thermally Driven Ag-Au Compositional Changes at the Ligament Surface in Nanoporous Gold: Implications for Electrocatalytic Applications. *ACS Appl. Nano Mater.* **2020**, *3*, 2197–2206. [\[CrossRef\]](#)
18. Xue, Y.; Scaglione, F.; Rizzi, P.; Battezzati, L. High performance SERS on nanoporous gold substrates synthesized by chemical de-alloying a Au-based metallic glass. *Appl. Surf. Sci.* **2017**, *426*, 1113–1120. [\[CrossRef\]](#)
19. Zhang, L.; Jing, Z.; Li, Z.; Fujita, T. Surface Defects Improved SERS Activity of Nanoporous Gold Prepared by Electrochemical Dealloying. *Nanomaterials* **2023**, *13*, 187. [\[CrossRef\]](#)
20. Chen, T.; Liu, X.; Zhao, L.; Hu, L.; Li, J.; Qu, F.; Le, G.; Qi, L.; Wang, X. Investigation on the two-stage hierarchical phase separation in the laser cladded Cu–Mn–Fe coating. *Vacuum* **2020**, *176*, 109331. [\[CrossRef\]](#)
21. Erlebacher, J.; Aziz, M.J.; Karma, A.; Dimitrov, N.; Sieradzki, K. Evolution of nanoporosity in dealloying. *Nature* **2001**, *410*, 450–453. [\[CrossRef\]](#)
22. Ge, X.B.; Chen, L.Y.; Kang, J.L.; Fujita, T.; Hirata, A.; Zhang, W.; Jiang, J.H.; Chen, M.W. A Core-Shell Nanoporous Pt-Cu Catalyst with Tunable Composition and High Catalytic Activity. *Adv. Funct. Mater.* **2013**, *23*, 4156–4162. [\[CrossRef\]](#)
23. Chen, N.; Frank, R.; Asao, N.; Louzguine-Luzgin, D.V.; Sharma, P.; Wang, J.Q.; Xie, G.Q.; Ishikawa, Y.; Hatakeyama, N.; Lin, Y.C.; et al. Formation and properties of Au-based nanograined metallic glasses. *Acta Mater.* **2011**, *59*, 6433–6440. [\[CrossRef\]](#)
24. Liu, X.; Chen, N.; Gu, J.L.; Du, J.; Yao, K.F. Novel Cu-Ag bimetallic porous nanomembrane prepared from a multi-component metallic glass. *RSC Adv.* **2015**, *5*, 50565–50571. [\[CrossRef\]](#)
25. Liu, X.; Du, J.; Shao, Y.; Zhao, S.F.; Yao, K.F. One-pot preparation of nanoporous Ag-Cu@Ag core-shell alloy with enhanced oxidative stability and robust antibacterial activity. *Sci. Rep.* **2017**, *7*, 10249. [\[CrossRef\]](#)
26. Liu, X.; Zhao, S.F.; Shao, Y.; Yao, K.F. Facile synthesis of air-stable nano/submicro dendritic copper structures and their anti-oxidation properties. *RSC Adv.* **2014**, *4*, 33362–33365. [\[CrossRef\]](#)
27. Liu, X.; Shao, Y.; Chen, N.; Zhao, S.; Du, J.; Li, J.; Le, G.-M.; Yao, K. Magical oxygen: Tuning Cu&Ag nanoporous membrane into nanoporous (Cu&Ag)@Ag core-shell alloy. *Phys. B Condens. Matter* **2021**, *614*, 413011.
28. Zhang, J.; Li, X.; Sun, X.; Li, Y. Surface Enhanced Raman Scattering Effects of Silver Colloids with Different Shapes. *J. Phys. Chem. B* **2005**, *109*, 12544–12548. [\[CrossRef\]](#)
29. Hildebrandt, P.; Stockburger, M. Surface-Enhanced Resonance Raman Spectroscopy of Rhodamine 6G adsorbed on colloidal silver. *J. Phys. Chem.* **1984**, *88*, 5935–5944. [\[CrossRef\]](#)
30. Niu, Z.Q.; Liu, H.M.; Chen, Y.; Gu, C.J.; Zhao, Z.Q.; Jiang, T. Sandwich Au/SMSiO<sub>2</sub>/Ag hybrid substrate: Synthesis, characterization, and surface-enhanced Raman scattering performance. *J. Nanopart. Res.* **2020**, *22*, 12. [\[CrossRef\]](#)
31. Chen, X.-H.; Zhu, J.; Li, J.-J.; Zhao, J.-W. A plasmonic and SERS dual-mode iodide ions detecting probe based on the etching of Ag-coated tetrapod gold nanostars. *J. Nanopart. Res.* **2019**, *21*, 158. [\[CrossRef\]](#)

**Disclaimer/Publisher's Note:** The statements, opinions and data contained in all publications are solely those of the individual author(s) and contributor(s) and not of MDPI and/or the editor(s). MDPI and/or the editor(s) disclaim responsibility for any injury to people or property resulting from any ideas, methods, instructions or products referred to in the content.